

Article

Plasma-Sputtered Growth of Ni-Pd Bimetallic Nanoparticles on Carbon Nanotubes for Toluene Sensing

Selene Acosta ¹, Juan Casanova-Chafer ^{2,3} , Eduard Llobet ³ , Axel Hemberg ⁴, Mildred Quintana ^{1,5} and Carla Bittencourt ^{2,*} 

- ¹ Centro de Investigación en Ciencias de la Salud y Biomedicina, Universidad Autónoma de San Luis Potosí, Av. Sierra Leona 550, Lomas de San Luis, San Luis Potosí 78210, Mexico; selene.acosta@uaslp.mx (S.A.); mildred.quintana@uaslp.mx (M.Q.)
- ² Chimie des Interactions Plasma Surface, Institute for Materials Science and Engineering, Université de Mons, Place du Parc 23, 7000 Mons, Belgium; juan.casanovachafer@umons.ac.be
- ³ Departament d'Enginyeria Electronica, Universitat Rovira i Virgili, Països Catalans 26, 43007 Tarragona, Spain; eduard.llobet@urv.cat
- ⁴ Materia Nova Research Center, 7000 Mons, Belgium; axel.hemberg@materianova.be
- ⁵ Facultad de Ciencias, Universidad Autónoma de San Luis Potosí, Av. Parque Chapultepec 1570, Privadas del Pedregal, San Luis Potosí 78295, Mexico
- * Correspondence: carla.bittencourt@umons.ac.be

Abstract: The properties of carbon nanotubes (CNTs) can be effectively tailored by decorating their surface with metal nanoparticles. For the decoration, first plasma functionalization is used to add oxygen chemical groups to the CNTs surface. Afterwards, the Ox-CNTs are decorated with Ni-Pd bimetallic nanoparticles using plasma sputtering deposition, a clean, fast, and environmentally friendly functionalization method. The grafted oxygen groups serve as nucleation sites for the growth of the bimetallic nanoparticles. Finally, the Ni-Pd nanoparticle-decorated CNTs are assessed as a sensing layer for the detection of toluene.

Keywords: carbon nanotubes; bimetallic nanoparticles; toluene sensors



Citation: Acosta, S.; Casanova-Chafer, J.; Llobet, E.; Hemberg, A.; Quintana, M.; Bittencourt, C. Plasma-Sputtered Growth of Ni-Pd Bimetallic Nanoparticles on Carbon Nanotubes for Toluene Sensing. *Chemosensors* **2023**, *11*, 328. <https://doi.org/10.3390/chemosensors11060328>

Academic Editor: Andrea Ponzoni

Received: 10 May 2023

Revised: 28 May 2023

Accepted: 31 May 2023

Published: 2 June 2023



Copyright: © 2023 by the authors. Licensee MDPI, Basel, Switzerland. This article is an open access article distributed under the terms and conditions of the Creative Commons Attribution (CC BY) license (<https://creativecommons.org/licenses/by/4.0/>).

1. Introduction

Recently, there has been an increasing need to develop sensors for different applications, including chemical, pressure, and temperature sensing [1–3]. Specifically, developing novel chemical sensors can help to solve problems involving environmental monitoring, medical diagnoses, and even space exploration [4]. For example, detecting toxic gases due to the global increase in air pollution is essential for detecting hazardous gas leakages that can harm the environment [5]. In this context, commercial chemical sensors must fulfill characteristics such as high selectivity and sensitivity, fast recovery and response, low power consumption, low-cost fabrication, portability, and stability [6]. In this direction, the use of nanomaterials as active materials in sensors has been raised as an important way to improve the sensing properties of commercial sensors or develop novel sensors due to properties such as large surface area, high sensitivity to changes in their electrical, chemical, and thermal properties, and exceptional mechanical properties.

Owing to their distinctive physical and electrical properties, carbon nanotubes (CNTs) have been extensively studied for their implementation in various applications, including chemical sensor devices [7,8]. CNTs have high thermal conductivity, chemical stability, and tensile strength [9,10]. These properties, combined with their large surface-to-volume ratio, promote optimal interactions with the target gas compounds, increase sensor sensitivity, and lower the detection limits. The basic principle of chemical sensing using CNTs as active materials towards electron-donating and acceptor molecules consists of charge transfer among the molecules and the p-type semiconducting CNTs. This charge transfer produces an enhancement or depletion of the charge carriers in the tubes, hence a monitorable change

in their electrical resistance [6,11]. The sensor's efficiency will depend on the effective adsorption and desorption processes of the gas molecules on the active material. Chemical sensing is based on the change in electrical properties (i.e., resistivity) of the active material. Therefore, chemical sensors are considered low-cost sensors, giving them an advantage over optical and physical sensors [5].

Despite the appropriate properties of pristine CNTs, some drawbacks still need to be improved for their optimal implementation in chemical sensors, such as poor sensitivity, selectivity, and long recovery times when operated at room temperature. Shorter recovery times can be reached when high operating temperatures (between 100 and 200 °C) are used [12], leading to high-power consumption and complex commercialization setups [13, 14]. To tackle these disadvantages, CNTs have been functionalized with several molecules, polymers, and nanoparticles to fine-tune their properties and create active sites on their surface [15]. In this sense, the CNTs' decoration with metal nanoparticles has been explored since adding noble metals to their surface has shown improved sensitivity towards certain gases [5]. For example, Mohsen Asad et al., observed an increased sensitivity of SWCNTs towards H₂S when their surface was decorated with Cu-nanoparticles [16]. Furthermore, functionalizing CNTs with metal nanoparticles generally leads to forming a composite material with higher strength, stiffness, and toughness, and with improved current carrying capabilities [17]. This synergy of CNTs and metal nanoparticle properties has pushed their application in catalysis, biological sensors, electronics, and energy storage devices [18–22].

Electrochemical methods are commonly used to decorate CNTs with metal nanoparticles. However, these techniques have the disadvantage of generating large amounts of liquid waste, requiring long-time treatments and low efficiency [23]. Conversely, methods such as ion beam deposition by irradiation, evaporation, or plasma sputtering are more advantageous because they are faster and more efficient. Furthermore, these methods are eco-friendly because they do not generate liquid waste [24–26]. Among these methods, plasma sputtering deposition is a commercial method used in microelectronics, coatings, metallurgy, and other applications [27]. Sputtering deposition consists of the ejection of atoms from a metal target using a bombardment of energetic particles which collide with atoms on the surface of the target, causing their ejection [28]. The energetic particles are usually ions produced by ion or plasma sources; ion sources are less common because they are more complex and expensive than plasma sources. In plasma sputtering deposition, the ions from the plasma are accelerated into a metal target using a negative voltage into the target; these ions have enough energy to eject metal atoms from the target. Then, sputtered atoms leave the target to collide with the surface of a substrate positioned on the opposite side of the target. In the case of metal nanoparticle formation, the metal atoms move along the substrate surface until they reach a nucleation point, forming clusters that then act as condensation centers to form nanoparticles [29].

The deposition of bimetallic nanoparticles onto the CNTs' surface has been raised as an alternative to enhance their sensing capabilities. It has been observed that the synergistic combination of metals can improve the composite stability, selectivity, and sensing performance if they are compared to monometallic nanoparticles [30]. However, the interactions between metals and the surface of graphite are reported to be weak due to the inert nature of *sp*² carbons. For this reason, it has been reported that *sp*² carbon materials, like CNTs, are functionalized with metal nanoparticles, mainly at the defect sites of their structures, which in the case of nanotubes are predominantly at the tips [29,31]. However, Felten et al., showed that introducing oxygen functional groups on CNTs, before the decoration of the CNTs with metal nanoparticles, employing oxygen plasma treatment leads to a more ubiquitous localization of the nanoparticles in the basal plane of the CNTs. This better distribution of the particles occurs because the oxygen groups grafted onto the CNTs surface serve as nucleation spots for the formation of the nanoparticles [31].

Herein, CNTs were first functionalized with oxygen groups, employing an oxygen plasma to create active sites for nanoparticle nucleation. Then, bimetallic Ni-Pd nanopar-

ticles were grown on CNTs, using the plasma sputtering deposition method. Finally, the obtained samples were evaluated as active materials in chemical sensors to detect toluene.

2. Materials and Methods

2.1. Bimetallic NPs Decoration of MWCNTs

Multi-walled carbon nanotubes (MWCNTs) were obtained from Nanocyl S. A. (Namur, Belgium). The average length of the MWCNTs was 50 μm , and the average inner and outer diameters were 3 and 15 nm, respectively. First, MWCNTs were dispersed in ethanol with a concentration of 0.1 mg/mL by sonication in a bath for 20 min. Afterward, the dispersion was airbrushed onto a commercial alumina substrate from Ceram Tech GmbH (Lohmar, Germany), which had screen-printed interdigitated platinum electrodes on one side and a screen-printed heater on the other side. Next, the MWCNTs were functionalized with oxygen groups by performing an oxygen plasma functionalization. The oxygen functionalization was performed in a plasma chamber with a residual pressure of 1.8×10^{-6} Torr. The discharge was produced by means of an advanced energy RF power generator with a power of 100 W. Then, a flow of O_2 (50 sccm) was put into the chamber with a working pressure of 7×10^{-4} Torr. The treatment time was 5 min. Then, for the decoration of MWCNTs with bimetallic NPs, plasma sputtering deposition was employed using palladium and nickel metal targets, respectively. The nanotubes were first decorated with palladium, and the sensor containing the oxygen-functionalized MWCNTs was located in the sputtering chamber, which was then brought to a pressure of 10^{-5} Torr. Afterwards, the pressure of the chamber was set to 25 mTorr using an argon flux with a flow of 20 sccm. Next, plasma was generated by initiating the magnetron power at 50 W. Palladium sputtering was performed for 5 s. This sputtering time permitted the production of a palladium film with an approximate thickness of 10 Å. Afterward, the samples were decorated with nickel atoms to create bimetallic nanoparticles. The nickel sputtering was carried out similarly to the palladium but using a nickel target and changing the magnetron power to 100 W. Three samples with increased nickel concentrations were obtained by changing the sputtering time to 5, 10, and 30 s.

2.2. Characterization

XPS measurements were carried out with a VERSAPROBE PHI 5000 from Physical Electronics (Tokyo, Japan) outfitted with a monochromatic Al K X-ray source. Each sample's core level spectra were captured with an energy resolution of 0.6 eV. In addition, Raman spectra were measured with a Micro-Raman system (Senterra Bruker Optik GmbH, Ettlingen, Germany) with a resolution of 3 cm^{-1} . Finally, the samples were analyzed with a field-emission scanning electron microscope (FESEM), Carl Zeiss AG—ULTRA 55.

2.3. Gas Sensing

For sensor development, commercially available (CeramTech (Plochingen, Germany), GmbH) alumina substrates, which comprised a pair of screen-printed, interdigitated platinum electrodes with a 300 μm electrode gap on the front side and a platinum resistive heater meander on the backside, were used. Figure S1 shows a picture of the front and back of the alumina substrates used.

For testing the sensors, they were installed inside a Teflon test chamber that was joined to a gas delivery system where the gas of interest could be mixed with pure air to reach the desired concentration inside the testing chamber. Afterwards, the resistance of the sensors was computed by making use of an HP 34972A Agilent multimeter (Santa Clara, CA, USA), and changes in the sensor resistance were recorded while the sensors were in contact with four different concentrations of the toluene gas (2.5, 5, 7, and 10 ppm). The sensors were exposed to the toluene gas for 5 min for each gas concentration, followed by 10 min exposure to pure air. The sensor's response was represented by $\Delta R/R_0$, where ΔR is the resistance change observed, and R_0 is the sensor's resistance in air.

3. Results and Discussion

First, the multiwall carbon nanotubes (CNTs), randomly deposited on the commercial alumina sensor substrate, were functionalized with oxygen groups [32]. From XPS analysis, it was observed that the atomic concentration of oxygen increased from 7.9 at. % in pristine CNTs to 22.1 at. % in oxygen-functionalized CNTs (inset Figure 1a); oxygen in pristine CNTs is associated with oxygen surface contamination during their synthesis and manipulation. The CNT oxygen functionalization could be observed by comparing the C 1s spectra before and after functionalization (Figure 1a). Photoelectrons ejected from carbon atoms bonded to oxygen atoms are considered the source of the C1s spectrum broadening observed at high binding energies following oxygen functionalization. Oxygen is more electronegative than carbon; hence, a positive charge was induced in carbon atoms bonded to oxygen, which changed the electron screening of their nucleus, increasing the binding energy of the electrons in the core levels. Then, the C 1s spectrum of Ox-CNTs was analyzed to further investigate the carbon atoms' chemical nature (Figure 1b). Several components were used to fit the C1s spectrum. The component at 284.4 eV (blue line) was associated with graphitic carbon with sp^2 hybridization, and the component at 285.0 eV (green line) corresponded to photoelectrons ejected from sp^3 hybridized carbon, considered defects in the graphitic structure. The three remaining components were assigned to carbon atoms linked to oxygen in three configurations. The components at 286.6 eV (pink line) corresponded to epoxide groups (C-O), the component at 287.5 eV (burgundy line) was assigned to carbonyl groups (C=O), and the component at 288.8 eV (navy line) to carboxyl groups (COOH); peak assignments were carried out using theoretical and experimental data reported elsewhere [33,34]. The C 1s analysis shows that three different oxygen groups were grafted at the CNTs surface using oxygen plasma functionalization.

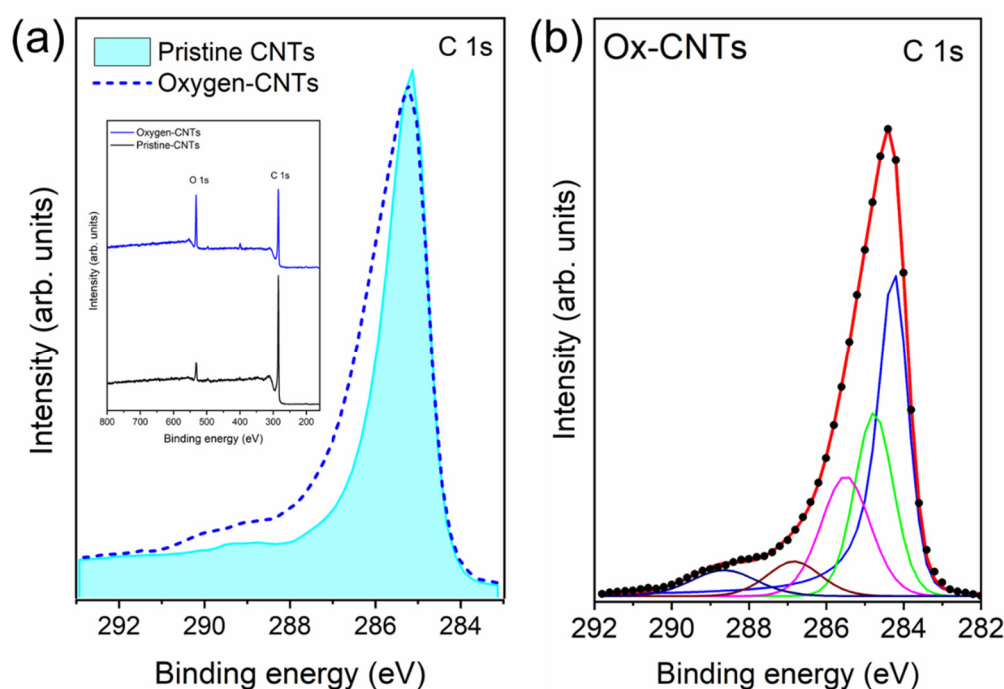


Figure 1. (a) C 1s XPS spectra of pristine and oxygen-functionalized CNTs. Inset: survey spectra of CNTs pristine (black) and Ox-CNTs (blue); (b) high-resolution C 1s XPS analysis spectrum of Ox-CNTs. Assignments: Red line → least square fitting result, blue line → C- sp^2 , green line → C- sp^3 , pink line → C-O, burgundy line → C=O, navy line → COOH. Black dots experimental data.

After oxygen functionalization, Ox-CNTs were decorated with bimetallic nickel–palladium nanoparticles using plasma sputtering deposition. First, Ox-CNTs were decorated with palladium. The sputtering time was five seconds, allowing the obtention of a palladium film with a nominal thickness of 10 Å. Afterwards, the Pd-Ox-CNTs were deco-

rated with nickel using three sputtering times (5, 10, and 30 s) to obtain Ni-Pd bimetallic NPs with different nickel atomic concentrations. X-ray photoelectron spectroscopy (XPS) was performed for each sample after each sputtering deposition.

The XPS analysis of the C 1s spectra after the deposition of palladium and nickel on the surface of the nanotubes is shown in Figure 2. For both cases, the same number of components as the Ox-CNTs sample was used to reproduce the spectra. The C1s XPS analysis spectrum of the CNTs sputtered with palladium is shown in Figure 2a. New components related to forming a Pd-C phase could not be observed; the photoelectrons emitted from carbons atoms in Pd carbides (PdC_x) had binding energy centered at 282.0 eV [35]. The inset in Figure 2a showed the survey XPS spectrum exhibiting a peak at 335.5 eV associated with palladium atoms on the CNTs surface with a relative atomic concentration of 2.2 % (Table S1). The nanoparticle formation was reported to be initiated by the mobility and diffusion of Pd atoms at the CNTs surface before reaching a nucleation center. In this case, the oxygen functional groups at the CNTs surface functioned as nucleation centers for the agglomeration of Pd atoms to form nanoparticles due to the strong interaction between palladium and oxygen atoms [31,36].

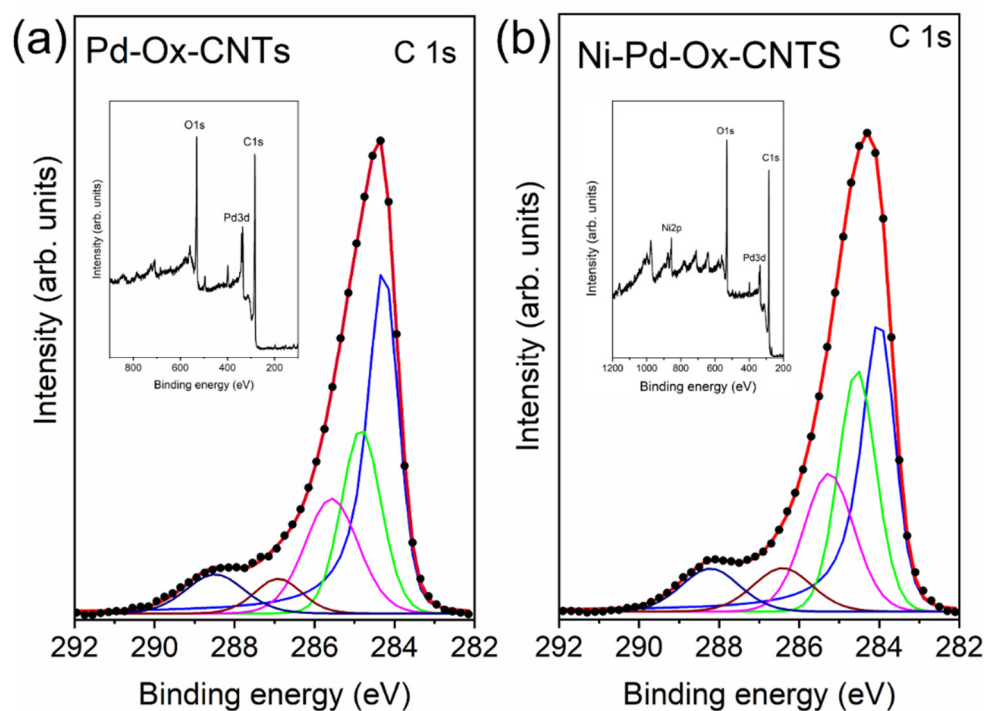


Figure 2. C 1s XPS analysis spectra of (a) Ox-CNTs after palladium deposition (Pd-Ox-CNTs); (b) Pd-Ox-CNTs after nickel deposition (Ni-Pd-Ox-CNTs). Insets: survey XPS spectra comparison between Pd-Ox-CNTs (a) and Ni-Pd-Ox-CNTs (b). Assignments: Red line → least square fitting result, blue line → C- sp^2 , green line → C- sp^3 , pink line → C-O, burgundy line → C=O, navy line → COOH. Black dots experimental data.

Consequently, oxygen functionalization promotes the formation of well-distributed metal NPs in the CNTs surface, as demonstrated by Felten and collaborators in 2009 [31]. Similarly, for the case of nickel sputtering onto Pd-Ox-CNTs, no new components were observed in the C 1s spectrum, demonstrating that Ni-C bonds were not formed. The inset in Figure 2b shows the survey spectrum with peaks created by photoelectrons ejected from palladium and nickel atoms on the CNTs surface at 335.5 eV and 855.8 eV, respectively.

The Pd 3d core-level XPS analysis spectra are shown in Figure 3. The Pd 3d spectrum recorded on the Pd-Ox-CNTs sample (Figure 3a) showed two doublets (Pd 3d $_{5/2}$, Pd 3d $_{3/2}$). The first doublet (blue lines) was centered at 336.1 and 341.4 eV of binding energies for Pd 3d $_{5/2}$ and Pd 3d $_{3/2}$, respectively. Therefore, this doublet was assigned to metallic Pd (Pd 0) [37]. The second doublet (green lines) had binding energies of 337.7 and 343.0 eV

and was associated with PdO (Pd^{2+}) [37]. The presence of Pd^{2+} corroborates the interaction of palladium with oxygen functional groups grafted at the surface of the tubes. This is consistent with the results reported by Felten and collaborators, where oxygen functionalizations work as nucleation sites for forming Pd nanoparticles [31]. Figure 3b–d show the Pd 3d XPS analysis spectra of the samples containing nickel; 5, 10, and 30 s nickel-sputtered samples, respectively. Compared to the sample containing only palladium, a third doublet was necessary to reproduce the Pd 3d spectra of the Ni-Pd samples. This doublet had binding energies of 338.0 and 343.3 eV (magenta lines) and was assigned to Pd^{3+} . This oxidation state was associated with two possible chemical environments of palladium, the further oxidation of palladium (PdO_x) or Pd atoms interacting with Ni atoms [37]. The highest relative concentration of this doublet was observed in the sample sputtered with nickel for 10 s. These results suggest that the nickel atoms diffuse on the CNTs surface until reaching an active site on the surface of CNTs, like oxygen functionalities or sites containing Pd-nanoparticles. Therefore, Ni-Pd bimetallic nanoparticles are formed. The formation of nanoparticle formation was verified using FESEM (Figure S2).

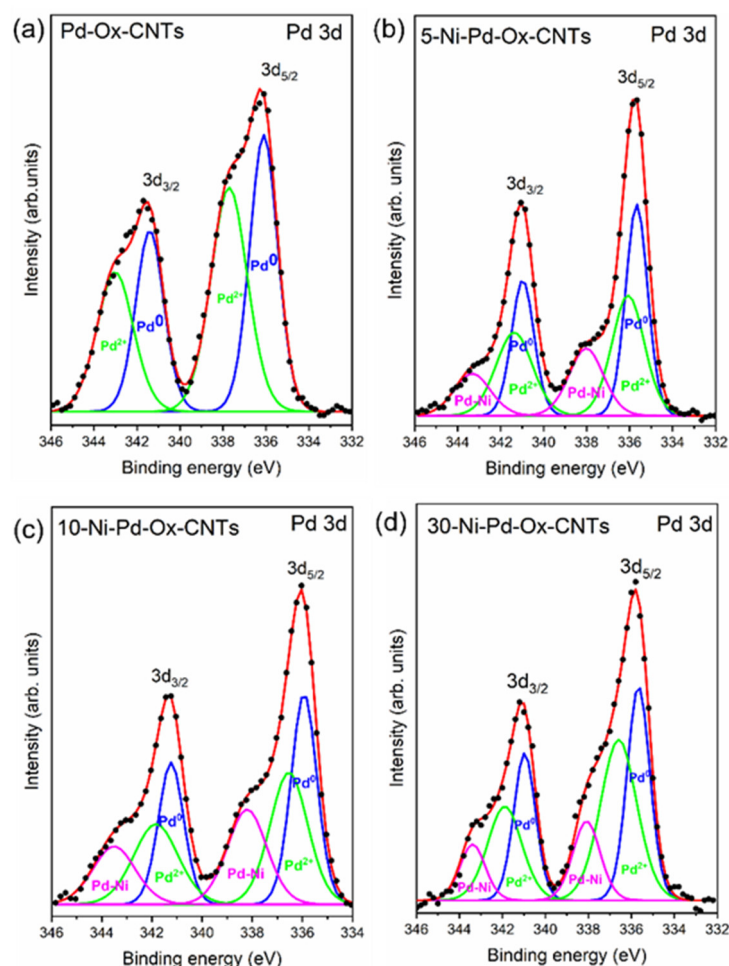


Figure 3. Pd 3d XPS analysis spectra. (a) Pd-Ox-CNTs; (b) 5Ni-Pd-Ox-CNTs; (c) 10Ni-Pd-Ox-CNTs; and (d) 30Ni-Pd-Ox-CNTs. The blue doublet is associated with d to Pd^0 , green doublet to Pd^{2+} , and pink doublet to PdO-NiO interactions, and the red line is the least square fitting result—black dots experimental data.

The analysis of the Ni 2p XPS spectra of the Ni-Pd-Ox-CNTs samples is shown in Figure 4. For simplicity, only the Ni $2p_{3/2}$ contribution is shown. Four components were used to reproduce the spectra of the three samples (5, 10, and 30 s of nickel sputtering) (Figure 4a–c). The component at 853.8 eV (cyan line) was associated with metallic nickel (Ni^0), the one at 855.9 eV was assigned to NiO (Ni^{2+}) (blue line), and a third component at

858.8 eV (navy line) was related to the further oxidation of nickel (Ni^{3+}). Finally, the broad component at 861.8 eV was associated with the shake-up satellite peak [38,39]. Although there was a small contribution of metallic nickel (Ni^0) on the surface of nanotubes, most of the nickel in the nanoparticles was oxidized (Ni^{2+} and Ni^{3+}). This correlates with the well-known high reactivity of nickel with oxygen atoms [37]. As expected, the relative concentration of nickel in the NPs increased when the sputtering time increased. The relative atomic concentration of nickel was 0.8 at. % for the 5-Ni-Pd-OxCNTs sample, 1.9 at. % for 10-Ni-Pd-OxCNTs, and 5.8 at. % for the 30-Ni-Pd-OxCNTs sample (Table S1).

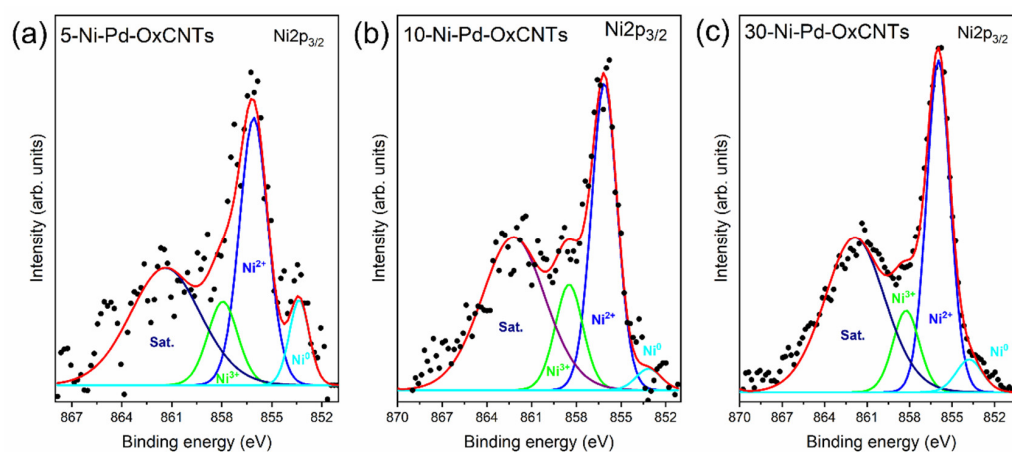


Figure 4. Ni $2p_{3/2}$ XPS analysis spectra. (a) 5Ni-Pd-Ox-CNTs; (b) 10Ni-Pd-Ox-CNTs; and (c) 30Ni-Pd-Ox-CNTs. The cyan component is related to Ni^0 , the blue component to Ni^{2+} , the green component to Ni^{3+} , the purple component belongs to the shake-up satellite peak, and the red line is the least square fitting result—black dots experimental data.

The presence of defects on carbon nanotubes after the plasma sputtering deposition of palladium and nickel was investigated using Raman spectroscopy (Figure 5). The analysis of the Raman spectra allowed the characterization of defects or disorder in the CNTs because the $C\text{-}sp^2$ environment affected the resonance Raman spectra of the tubes [40]. Therefore, these spectra permit investigating the effect in the $C\text{-}sp^2$ environment of growing palladium and nickel–palladium nanoparticles on Ox-CNTs. The characteristic Raman peaks of carbon nanotubes are shown in Figure 5, where the G band located at 1580 cm^{-1} is related to the graphitic sp^2 structure, and the D band at 1350 cm^{-1} is associated with the loss of symmetry in the sp^2 configuration due to the presence of disorder [40]. Figure 5a compares the Raman spectra of Ox-CNTs (blue) and Pd-Ox-CNTs (black). No significant changes were observed. The D peak intensity associated with the disorder in CNTs showed no increase after sputtering palladium onto the CNTs surface. The Raman spectra verified the XPS findings, where C-Pd bonds were not identified. Similarly, the Raman spectra of carbon nanotubes containing Ni-Pd nanoparticles showed that the formation of the nanoparticles did not induce further disorder in the structure of the carbon nanotubes (Figure 5b).

Finally, the synthesized samples of Pd-Ox-CNTs and Ni-Pd-Ox-CNTs were assessed as active layers in chemical sensors to detect toluene (Figure 6). Toluene is a contaminant present in the incomplete combustion of gasoline vehicles, and its inhalation affects the nervous system, heart, and liver [41]. Thus, developing sensors to supervise toluene gas in trace levels is necessary as these sensors can be used to optimize combustion processes. Figure 6a shows the active layers' resistance variation when exposed to different increasing ppm concentrations of toluene (2.5, 5, 7, and 10 ppm) at room temperature (RT) measurements. The four types of sensors tested showed a different resistance in air: $74\ \Omega$ for Pd-Ox-CNTs, $75\ \Omega$ for 5-Ni-Pd-Ox-CNTs, $53\ \Omega$ for 10-NiPd-Ox-CNTs, and $83\ \Omega$ for 30-Ni-Pd-Ox-CNTs. The resistance of the active layers increased after their exposure to toluene due to the charge transfer from toluene molecules to the Ox-CNTs. Curves in

Figure 6a showed adequate recovery of the resistance baseline after exposure to toluene, indicating effective toluene desorption from the Ox-CNTs active layer. Figure 6b shows the calibration curves for the four types of sensors tested (the linear equations are detailed in Table S2). A better response for the case of the 5-Ni-Pd-Ox-CNTs sample at lower toluene concentrations can be observed. This indicates that bimetallic nanoparticles may synergistically affect Ni-Pd-Ox-CNT sensors when they have a small nickel concentration. Figure 6a,b shows that the 5-Ni-Pd-Ox-CNTs sample had a higher efficiency in sensing toluene than others. Afterwards, increasing the nickel content in the 10-Ni-Pd-Ox-CNTs led to a dropping in this efficiency. Then, the 30-Ni-Pd-Ox-CNTs, which had the highest concentration of nickel, presented a recovery of the sensing efficiency. Correlating these results with the XPS analysis of the samples, it can be suggested that the relative concentration of metallic nickel (Ni^0) affects the efficiency of the sensors. Figure 4 and Table S3 show that the 5-Ni-Pd-Ox-CNTs sample had the highest relative concentration of metallic nickel. Then, this concentration decreased in the 10-Ni-Pd-Ox-CNTs and increased again in 30-Ni-Pd-Ox-CNTs, therefore indicating that metallic nickel may have a stronger interaction with toluene molecules than Ni^{2+} or Ni^{3+} , leading to the increased adsorption of toluene in 5-Ni-Pd nanoparticles and, subsequently, to an increased response for the 5-Ni-Pd-Ox-CNTs active layer to sense toluene. To evaluate the selectivity of the active layers towards toluene, these were also tested to detect H_2 , NO_2 , and ethanol at room temperature. The curve responses are shown in Figure S3. Although several active layers showed no response to these gases, some offered a change in the resistance in the presence of H_2 , NO_2 , and ethanol. These results suggest that the selectivity of these materials can still be improved.

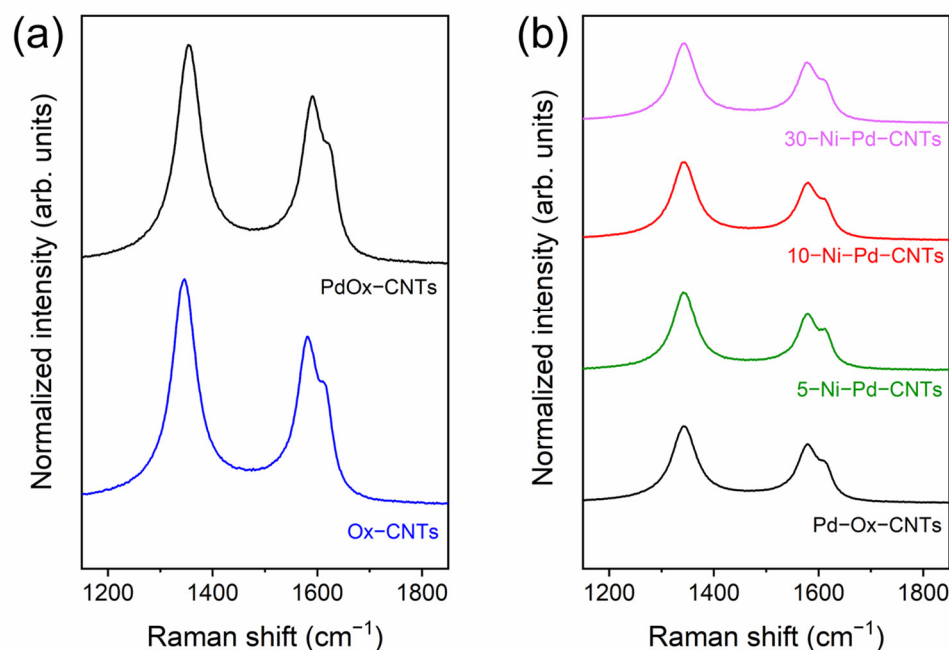


Figure 5. Raman spectra comparison of CNTs samples. (a) Ox-CNTs and Pd-Ox-CNTs; (b) Pd-Ox-CNTs and Ni-Pd-Ox-CNTs.

The interactions between toluene, metallic nanoparticles, and Ox-CNTs are key to the sensing mechanism for Pd-Ox-CNTs and Ni-Pd-Ox-CNTs towards toluene. Pd/Ni-loaded CNTs showed a higher response to toluene than to any other gaseous species tested (Figure S3). Aromatic VOCs can be detected by CNT films via π - π interactions (i.e., the stacking of the aromatic ring onto the outer wall of CNTs) [42]. However, π - π interactions involve a very limited charge transfer between the adsorbed molecule and the CNT film, which results in small responses. The use of catalyst bimetallic nanoparticles, i.e., Pd-M (M = Pt, Ni, Cu, Co) supported on SiO_2 , has been investigated for the hydrogenation reaction

of benzene and toluene. It was found that the Pd-Ni system showed the highest turnover frequencies for benzene and toluene hydrogenation. This effect could be attributed to the large amount of electron-deficient Pd δ^+ sites located on the surface of Pd-Ni. These sites greatly favor the adsorption of electron-rich benzene and toluene molecules [43]. In addition, Pd-Ni catalysts supported on SiO₂ showed good stability and reusability without a significant decrease in their catalytic activity after many runs. Therefore, the main reason for the improvement in toluene response brought about by the Pd-Ni loading of CNTs may be due to the enhancement in the toluene adsorption capacity and the associated electronic charge injection from adsorbed molecules towards the Pd-Ni/CNT film.

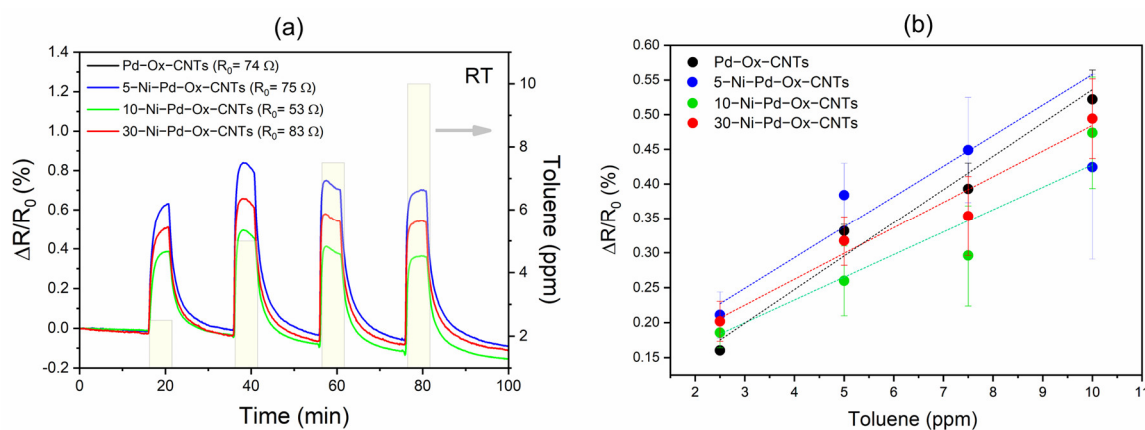


Figure 6. (a) Response and recovery curves of Pd-Ox-CNTs and Ni-Pd-Ox-CNT active layers in response to variable concentrations of toluene; (b) Calibration curves of Pd-Ox-CNTs and Ni-Pd-Ox-CNT active layers. The measurements were carried out at room temperature.

4. Conclusions

Carbon nanotubes were first functionalized with oxygen groups via oxygen plasma functionalization, a fast, clean, and efficient technique. This method achieved a remarkable 22.1% oxygen atomic concentration after only 5 min of functionalization. The presence of epoxide (C-O), carbonyl (C=O), and carboxyl (COOH) groups was confirmed through XPS analysis. Afterwards, it was demonstrated that the oxygen functionalities grafted at the CNTs basal plane acted as nucleation spots for forming Pd and Ni-Pd nanoparticles. Significantly, decorating CNTs with the nanoparticles did not increase the disorder in the nanotubes' structure. Finally, the Pd- and Ni-Pd-decorated Ox-CNTs were evaluated as active layers to sense toluene. The sample containing 5-Ni-Pd bimetallic nanoparticles showed superior performance, suggesting a possible synergy of the metallic Ni properties. However, further investigations are needed to completely comprehend the function of the relative nickel concentration in the Ni-Pd nanoparticles in detecting toluene and other gases.

Supplementary Materials: The following supporting information can be downloaded at: <https://www.mdpi.com/article/10.3390/chemosensors11060328/s1>, Figure S1: Commercially alumina substrates (CeramTech, GmbH) used for gas sensing tests; Figure S2: FESEM images of 5-Ni-Pd-OxCNTs (a) and 30-Ni-Pd-OxCNTs (b). Bright spots reveal the presence of bimetallic nanoparticles; Table S1: Relative atomic concentration of elements on CNTs samples before and after deposition of Pd and Ni-Pd nanoparticles. Data obtained from XPS analysis; Figure S3: Response and recovery curves of Pd-Ox-CNTs and Ni-Pd-Ox-CNT active layers for a variable concentration of (a) H₂; (b) NO₂; (c) Ethanol. The measurements were carried out at room temperature. The samples not shown in each graph did not respond to that specific gas; Table S2. Linear equations for the calibration curves for the four sensors tested. Table S3. FWHM and position of the components used to reproduce the Ni2p spectra. %relative contribution to the peak intensity.

Author Contributions: Conceptualization, E.L., M.Q. and C.B.; methodology, S.A. and J.C.-C.; validation, S.A. and J.C.-C.; formal analysis, S.A.; investigation, S.A., J.C.-C., A.H. and C.B.; resources, C.B., A.H., M.Q. and E.L.; writing—original draft preparation, S.A.; writing—review and editing, J.C.-C. and C.B.; visualization, C.B.; supervision, E.L., C.B. and M.Q. All authors have read and agreed to the published version of the manuscript.

Funding: This research received no external funding.

Institutional Review Board Statement: Not applicable.

Informed Consent Statement: Not applicable.

Data Availability Statement: Not applicable.

Acknowledgments: E.L. is supported by the Catalan Institute for advanced studies (ICREA) via the 2018 Edition of the ICREA Academia Award. C.B. is a Research Associate of the FRS-FNRS, Belgium. C.B. thanks the Belgian Fund for Scientific Research under the FRFC contract EQP 40002995 (PHOTOFUN). J.C.-C. is supported by the Marie Skłodowska-Curie grant agreement No. 101066282—GREBOS.

Conflicts of Interest: The authors declare no conflict of interest. The funders had no role in the design of the study; in the collection, analyses, or interpretation of data; in the writing of the manuscript; or in the decision to publish the results.

References

1. Schroeder, V.; Savagatrup, S.; He, M.; Lin, S.; Swager, T.M. Carbon Nanotube Chemical Sensors. *Chem. Rev.* **2019**, *119*, 599–663. [[CrossRef](#)] [[PubMed](#)]
2. Song, P.; Ma, Z.; Ma, J.; Yang, L.; Wei, J.; Zhao, Y.; Zhang, M.; Yang, F.; Wang, X. Recent Progress of Miniature MEMS Pressure Sensors. *Micromachines* **2020**, *11*, 56. [[CrossRef](#)] [[PubMed](#)]
3. Bhar, I.; Mandal, N. A Review on Advanced Wireless Passive Temperature Sensors. *Measurement* **2022**, *187*, 110255. [[CrossRef](#)]
4. Mehrotra, P. Biosensors and Their Applications—A Review. *J. Oral Biol. Craniofacial Res.* **2016**, *6*, 153–159. [[CrossRef](#)]
5. Young, S.-J.; Liu, Y.-H.; Lin, Z.-D.; Ahmed, K.; Shiblee, M.N.I.; Romanuik, S.; Sekhar, P.K.; Thundat, T.; Nagahara, L.; Arya, S.; et al. Multi-Walled Carbon Nanotubes Decorated with Silver Nanoparticles for Acetone Gas Sensing at Room Temperature. *J. Electrochem. Soc.* **2020**, *167*, 167519. [[CrossRef](#)]
6. Kumar, S.; Pavelyev, V.; Mishra, P.; Tripathi, N. A Review on Chemiresistive Gas Sensors Based on Carbon Nanotubes: Device and Technology Transformation. *Sens. Actuators A Phys.* **2018**, *283*, 174–186. [[CrossRef](#)]
7. Rasheed, T.; Nabeel, F.; Adeel, M.; Rizwan, K.; Bilal, M.; Iqbal, H.M.N. Carbon Nanotubes-Based Cues: A Pathway to Future Sensing and Detection of Hazardous Pollutants. *J. Mol. Liq.* **2019**, *292*, 111425. [[CrossRef](#)]
8. Yao, X.; Zhang, Y.; Jin, W.; Hu, Y.; Cui, Y. Carbon Nanotube Field-Effect Transistor-Based Chemical and Biological Sensors. *Sensors* **2021**, *21*, 995. [[CrossRef](#)]
9. Kim, P.; Shi, L.; Majumdar, A.; McEuen, P.L. Thermal Transport Measurements of Individual Multiwalled Nanotubes. *Phys. Rev. Lett.* **2001**, *87*, 215502. [[CrossRef](#)]
10. Wong, E.W.; Sheehan, P.E.; Lieber, C.M. Nanobeam Mechanics: Elasticity, Strength, and Toughness of Nanorods and Nanotubes. *Science* **1997**, *277*, 1971–1975. [[CrossRef](#)]
11. Hua, C.; Shang, Y.; Wang, Y.; Xu, J.; Zhang, Y.; Li, X.; Cao, A. A Flexible Gas Sensor Based on Single-Walled Carbon Nanotube-Fe₂O₃ Composite Film. *Appl. Surf. Sci.* **2017**, *405*, 405–411. [[CrossRef](#)]
12. Norizan, M.N.; Moklis, M.H.; Ngah Demon, S.Z.; Halim, N.A.; Samsuri, A.; Mohamad, I.S.; Knight, V.F.; Abdullah, N. Carbon Nanotubes: Functionalisation and Their Application in Chemical Sensors. *RSC Adv.* **2020**, *10*, 43704–43732. [[CrossRef](#)]
13. Sayago, I.; Santos, H.; Horrillo, M.C.; Alexandre, M.; Fernández, M.J.; Terrado, E.; Tacchini, I.; Aroz, R.; Maser, W.K.; Benito, A.M.; et al. Carbon Nanotube Networks as Gas Sensors for NO₂ Detection. *Talanta* **2008**, *77*, 758–764. [[CrossRef](#)]
14. Naje, A.N.; Ibraheem, R.R.; Ibrahim, F.T. Parametric Analysis of NO₂ Gas Sensor Based on Carbon Nanotubes. *Photonic Sens.* **2016**, *6*, 153–157. [[CrossRef](#)]
15. Han, T.; Nag, A.; Chandra Mukhopadhyay, S.; Xu, Y. Carbon Nanotubes and Its Gas-Sensing Applications: A Review. *Sens. Actuators A Phys.* **2019**, *291*, 107–143. [[CrossRef](#)]
16. Asad, M.; Sheikhi, M.H.; Pourfath, M.; Moradi, M. High Sensitive and Selective Flexible H₂S Gas Sensors Based on Cu Nanoparticle Decorated SWCNTs. *Sens. Actuators B Chem.* **2015**, *210*, 1–8. [[CrossRef](#)]
17. Subramaniam, C.; Yamada, T.; Kobashi, K.; Sekiguchi, A.; Futaba, D.N.; Yumura, M.; Hata, K. One Hundred Fold Increase in Current Carrying Capacity in a Carbon Nanotube–Copper Composite. *Nat. Commun.* **2013**, *4*, 2202. [[CrossRef](#)]
18. Panzer, M.A.; Zhang, G.; Mann, D.; Hu, X.; Pop, E.; Dai, H.; Goodson, K.E. Thermal Properties of Metal-Coated Vertically Aligned Single-Wall Nanotube Arrays. *J. Heat Transfer.* **2008**, *130*, 052401. [[CrossRef](#)]
19. Cross, R.; Cola, B.A.; Fisher, T.; Xu, X.; Gall, K.; Graham, S. A Metallization and Bonding Approach for High Performance Carbon Nanotube Thermal Materials. *Nanotechnology* **2010**, *21*, 445705. [[CrossRef](#)]

20. Bult, J.; Sawyer, W.G.; Voevodin, A.; Muratore, C.; Dickrell, P.; Pal, S.; Ajayan, P.; Schadler, L. Electrical Switching Using Compliant Metal Infiltrated Multi-Wall Nanotube Arrays. *MRS Online Proc. Libr.* **2008**, *1085*, 1085-T02-05. [[CrossRef](#)]
21. Somani, P.R.; Somani, S.P.; Umeno, M. Application of Metal Nanoparticles Decorated Carbon Nanotubes in Photovoltaics. *Appl. Phys. Lett.* **2008**, *93*, 033315. [[CrossRef](#)]
22. Claussen, J.C.; Franklin, A.D.; Haque, A.U.; Marshall Porterfield, D.; Fisher, T.S. Electrochemical Biosensor of Nanocube-Augmented Carbon Nanotube Networks. *ACS Nano* **2009**, *3*, 37–44. [[CrossRef](#)] [[PubMed](#)]
23. Wildgoose, G.G.; Banks, C.E.; Compton, R.G. Metal Nanoparticles and Related Materials Supported on Carbon Nanotubes: Methods and Applications. *Small* **2006**, *2*, 182–193. [[CrossRef](#)] [[PubMed](#)]
24. Janas, D.; Koziol, K.K.K. The Influence of Metal Nanoparticles on Electrical Properties of Carbon Nanotubes. *Appl. Surf. Sci.* **2016**, *376*, 74–78. [[CrossRef](#)]
25. Rabat, H.; Andreatza, C.; Brault, P.; Caillard, A.; Béguin, F.; Charles, C.; Boswell, R. Carbon/Platinum Nanotextured Films Produced by Plasma Sputtering. *Carbon* **2009**, *47*, 209–214. [[CrossRef](#)]
26. Chen, Q.; Zhang, Y.; Yang, L.; Chen, S.; Weng, J.; Yue, L. Polymer Driven Covalently Bonded Decahedral-Twinning of Ag Nanoparticles Prepared by ICP Enhanced Magnetron Sputtering Method. *J. Phys. Chem. C* **2009**, *113*, 7633–7638. [[CrossRef](#)]
27. Window, B. Recent Advances in Sputter Deposition. *Surf. Coat. Technol.* **1995**, *71*, 93–97. [[CrossRef](#)]
28. Depla, D.; Mahieu, S.; Greene, J.E. Sputter Deposition Processes. In *Handbook of Deposition Technologies for Films and Coatings: Science, Applications and Technology*; William Andrew Publishing: Norwich, NY, USA, 2010; pp. 253–296. [[CrossRef](#)]
29. Zhang, Y.; Franklin, N.W.; Chen, R.J.; Dai, H. Metal Coating on Suspended Carbon Nanotubes and Its Implication to Metal–Tube Interaction. *Chem. Phys. Lett.* **2000**, *331*, 35–41. [[CrossRef](#)]
30. Fang, Y.L.; Miller, J.T.; Guo, N.; Heck, K.N.; Alvarez, P.J.J.; Wong, M.S. Structural Analysis of Palladium-Decorated Gold Nanoparticles as Colloidal Bimetallic Catalysts. *Catal. Today* **2011**, *160*, 96–102. [[CrossRef](#)]
31. Felten, A.; Ghijsen, J.; Pireaux, J.-J.; Drube, W.; Johnson, R.L.; Liang, D.; Hecq, M.; van Tendeloo, G.; Bittencourt, C. Electronic Structure of Pd Nanoparticles on Carbon Nanotubes. *Micron* **2009**, *40*, 74–79. [[CrossRef](#)]
32. Lobo, A.O.; Ramos, S.C.; Antunes, E.F.; Marciano, F.R.; Trava-Airoldi, V.J.; Corat, E.J. Fast Functionalization of Vertically Aligned Multiwalled Carbon Nanotubes Using Oxygen Plasma. *Mater. Lett.* **2012**, *70*, 89–93. [[CrossRef](#)]
33. Acosta, S.; Casanova Chafer, J.; Sierra Castillo, A.; Llobet, E.; Snyders, R.; Colomer, J.-F.; Quintana, M.; Ewels, C.; Bittencourt, C. Low Kinetic Energy Oxygen Ion Irradiation of Vertically Aligned Carbon Nanotubes. *Appl. Sci.* **2019**, *9*, 5342. [[CrossRef](#)]
34. Bittencourt, C.; Navio, C.; Nicolay, A.; Ruelle, B.; Godfroid, T.; Snyders, R.; Colomer, J.-F.; Lagos, M.J.; Ke, X.; van Tendeloo, G.; et al. Atomic Oxygen Functionalization of Vertically Aligned Carbon Nanotubes. *J. Phys. Chem. C* **2011**, *115*, 20412–20418. [[CrossRef](#)]
35. Han, Y.-F.; Kumar, D.; Sivadinarayana, C.; Clearfield, A.; Goodman, D.W. The Formation of Pd_x over Pd-Based Catalysts in Vapor-Phase Vinyl Acetate Synthesis: Does a Pd–Au Alloy Catalyst Resist Carbide Formation? *Catal. Lett.* **2004**, *94*, 131–134. [[CrossRef](#)]
36. Cai, Y.Q.; Bradshaw, A.M.; Guo, Q.; Goodman, D.W. The Size Dependence of the Electronic Structure of Pd Clusters Supported on Al₂O₃/Re(0001). *Surf. Sci.* **1998**, *399*, L357–L363. [[CrossRef](#)]
37. Luna, A.L.; Dragoe, D.; Wang, K.; Beaunier, P.; Kowalska, E.; Ohtani, B.; Bahena Uribe, D.; Valenzuela, M.A.; Remita, H.; Colbeau-Justin, C. Photocatalytic Hydrogen Evolution Using Ni–Pd/TiO₂: Correlation of Light Absorption, Charge-Carrier Dynamics, and Quantum Efficiency. *J. Phys. Chem. C* **2017**, *121*, 14302–14311. [[CrossRef](#)]
38. Xiong, D.; Li, W.; Liu, L. Vertically Aligned Porous Nickel(II) Hydroxide Nanosheets Supported on Carbon Paper with Long-Term Oxygen Evolution Performance. *Chem. Asian J.* **2017**, *12*, 543–551. [[CrossRef](#)]
39. Cheng, M.; Fan, H.; Song, Y.; Cui, Y.; Wang, R. Interconnected Hierarchical NiCo₂O₄ Microspheres as High-Performance Electrode Materials for Supercapacitors. *Dalton Trans.* **2017**, *46*, 9201–9209. [[CrossRef](#)]
40. Dresselhaus, M.S.; Jorio, A.; Souza Filho, A.G.; Saito, R. Defect Characterization in Graphene and Carbon Nanotubes Using Raman Spectroscopy. *Philos. Trans. R. Soc. A Math. Phys. Eng. Sci.* **2010**, *368*, 5355–5377. [[CrossRef](#)]
41. Kwon, Y.J.; Na, H.G.; Kang, S.Y.; Choi, S.-W.; Kim, S.S.; Kim, H.W. Selective Detection of Low Concentration Toluene Gas Using Pt-Decorated Carbon Nanotubes Sensors. *Sens. Actuators B Chem.* **2016**, *227*, 157–168. [[CrossRef](#)]
42. Clément, P.; Korom, S.; Struzzi, C.; Parra, E.J.; Bittencourt, C.; Ballester, P.; Llobet, E. Benzene Detection: Deep Cavitand Self-Assembled on Au NPs-MWCNT as Highly Sensitive Benzene Sensing Interface. *Adv. Funct. Mater.* **2015**, *25*, 4172. [[CrossRef](#)]
43. Yang, J.; Fan, Y.; Li, Z.-L.; Peng, Z.; Yang, J.-H.; Liu, B.; Liu, Z. Bimetallic Pd-M (M = Pt, Ni, Cu, Co) nanoparticles catalysts with strong electrostatic metal-support interaction for hydrogenation of toluene and benzene. *Mol. Catal.* **2020**, *492*, 110992. [[CrossRef](#)]

Disclaimer/Publisher’s Note: The statements, opinions and data contained in all publications are solely those of the individual author(s) and contributor(s) and not of MDPI and/or the editor(s). MDPI and/or the editor(s) disclaim responsibility for any injury to people or property resulting from any ideas, methods, instructions or products referred to in the content.